RSC Advances

Polyaniline-RuO2 composite for high performance supercapacitor: Chemical synthesis and properties

Journal:	*RSC Advances*
Manuscript ID:	RA-ART-12-2014-016969.R1
Article Type:	Paper
Date Submitted by the Author:	16-Feb-2015
Complete List of Authors:	Deshmukh, Prashant; Shivaji University Kolhapur, Department of Physics Bulakhe, Ravindra; Shivaji University, Kolhapur, Department of Physics Pusawale, Swati; Shivaji University, Kolhapur, Department of Physics Sartale, Shrikrishna; Savitribai Phule Pune University, Department of Physics Lokhande, Chandrakant; Shivaji University, Kolhapur, Department of Physics

Polyaniline-RuO_2 composite for high performance supercapacitor: Chemical synthesis and properties

P. R. Deshmukh[a], R. N. Bulakhe[a], S. N. Pusawale[a], S. D. Sartale[b] and C. D. Lokhande[a]*

[a] Thin Film Physics Laboratory, Department of Physics, Shivaji University, Kolhapur- 416 004 (M. S.) India.

[b] Department of Physics, Savitribai Phule Pune University, Pune - 411 007 (M. S.) India.

Abstract

Composite thin films of polyaniline-ruthenium oxide (PANI-RuO_2) are prepared by a chemical bath deposition (CBD) method. The prepared thin films are characterized by X-ray diffraction (XRD), Fourier transform infrared (FT-IR) and FT-Raman spectroscopy. XRD patterns reveal amorphous nature of composite thin films. FT-IR and FT-Raman confirms PANI-RuO_2 composite formation. Cyclic voltammetry, galvanostatic charge–discharge and impedance analysis are carried out in order to investigate the applicability of the composite electrode as a supercapacitor. The PANI–RuO_2 composite electrode demonstrates the maximum specific capacitance of 830 Fg^{-1}. The specific energy and specific power of PANI-RuO_2 composite electrode are of 216 $Whkg^{-1}$ and 4.16 $kWkg^{-1}$, respectively. The observed specific capacitance is the best yet reported for PANI-RuO_2 composite supercapacitor in H_2SO_4 electrolyte. Moreover, the composite electrode shows enhanced cycling stability. These results demonstrate the potential of developing PANI-RuO_2 composite electrode material for high-performance supercapacitor.

Keywords: Chemical Synthesis, Thin films, FT-IR, Polymers, Oxides, Composite Materials.

*Corresponding author: Prof. C. D. Lokhande, E-mail address: l_chandrakant@yahoo.com Tel.: +91 231 2609225, Fax: +91 231 2692333.

1. Introduction

In response to the rapid development of the global economy, the exhaustion of fossil fuels and the environmental contamination, there is tremendous need to develop renewable, highly efficient methods of creating and storing energy without damaging the environment. It has stimulated recent advances in new clean source as well as technology associated with electrochemical energy storage i.e. supercapacitor. In particular, supercapacitors have increasingly attracted intense research attention due to their high power density, long cycle lifetime, and spanning function between traditional dielectric capacitors with high power output and batteries with high energy storage **[1, 2]**. It is vital to make greater efforts to design and synthesize novel materials for supercapacitor electrodes to pursue the above aspects. Porous carbons, transition metal oxides, and conducting polymers are fundamental candidates for supercapacitor electrode materials **[3]**. However, metal oxides and conducting polymers are

disturbed by several key drawbacks. For example, metal oxides are expensive (RuO_2) or poorly conductive (NiO, MnO_2, etc.); and conducting polymers show short cycling life **[4, 5]**.

To overcome the drawback of individual supercapacitive material, formation of composite materials may be the possible customs. Therefore many researchers have moved towards the formation of composite materials of polymers and metal oxides since the dramatic improvements in their properties and performances can be achieved due to the synergistic effect between the two components **[6]**. Composites are a special class of materials originating from combinations of two or more compounds by a suitable technique, which results in materials having unique physiochemical properties and large potential application in diverse areas. The polymer composite material differs from the pure polymer in respect to some of the physical and chemical properties and hence it is useful for many applications in different fields **[7]**. Lin et al. electrochemically synthesized PANI on thermally prepared RuO_2 using cyclic voltammetry technique **[8]**. Sopcic et al. fabricated PANI-RuO_2 composite by depositing PANI layer on RuO_2 surface demonstrating the enhancement in specific capacitance **[9]**. Recently, Shaikh et al. synthesized PANI-$HRuO_2$ composite material using electrodeposition technique **[10].** Hydrous Ru-oxide, as well as PANI has already been found as electroactive materials of primary interest for application in supercapacitor **[11, 12].** Both materials exhibit high specific capacitance by storing high quantity of charge through almost reversible redox capacitive mechanism. Because of high demand on electroactive materials with extremely high specific capacitances, an attempt is made to prepare, characterize PANI-RuO_2 composite films and to evaluate their performance in supercapacitor application.

In this study, PANI-RuO_2 composite thin films are synthesized and the amended supercapacitive properties are examined. However, to the best of our knowledge no study has been reported on supercapacitor properties of PANI-RuO_2 composite electrode using Chemical bath deposition (CBD) method. The PANI-RuO_2 composite electrodes are characterized by cyclic voltammetry, galvanostatic charge-discharge and electrochemical impedance spectroscopy techniques. Here, PANI-RuO_2 composite electrode exhibits increased capacitance in comparison with capacitance of pristine PANI. This shows that feasibility of CBD method as well as composite electrode towards the supercapacitor application.

2 Experimental Sections

2.1 Preparation of PANI

The chemical polymerization of aniline monomer was carried out at room temperature. In typical synthesis, 0.2 M aniline monomer was added in the 1 M H_2SO_4 solution. The stainless steel substrates were placed in the solution, in order to deposit PANI thin film

ammonium persulfate (0.1 M) as an oxidizing agent was added in the aniline solution. The thin PANI coating of 0.13 $mg.cm^{-2}$ thickness was observed after 30 minute of polymerization. The thickness obtained was not sufficient for the supercapacitive study. Therefore, we have repeated same process for four times. In this case, the maximum thickness of 0.24 $mg.cm^{-2}$ was observed after the third deposition.

2.2 Preparation of PANI-RuO_2 composite

Composites were prepared by chemical polymerization of aniline in mixed solution of aniline monomer and ruthenium chloride**. Fig. 1** shows the schematic presentation of CBD method for the synthesis of PANI-RuO_2 composite thin films. Preparation of PANI-RuO_2 composite thin film is based on the polymerization of aniline monomer and precipitation of ruthenium (III) chloride. The aniline solution was prepared using 0.2 M aniline monomer dissolved in 1 M H_2SO_4 **(Fig. 1 (a)).** The ruthenium chloride solution was prepared using 0.01 M $RuCl_3.xH_2O$ in double distilled water **(Fig. 1 (b)).** The prepared aniline and $RuCl_3$ solution (each of 30 ml) were mixed in another beaker **(Fig.1 (c)).** The clean and polished stainless steel substrates were vertically immersed in this solution **(Fig.1 (c))**. Then, an oxidant of 0.1 M ammonium persulfate (APS) was added to this mixed solution. Here, APS initiates the aniline monomer for polymerization. During the chemical reaction, clusters of PANI are covered by thin layers of RuO_2 depositing on the substrate as shown in **Fig. 1 (d).** The substrates coated with thin layer of PANI-RuO_2 composite were removed after 30 minute. The PANI-RuO_2 composite thin films were washed with double distilled water and air dried. The thickness obtained was 0.033 $mg.cm^{-2}$. This process was repeated for three times, since the maximum thickness of 0.12 $mg.cm^{-2}$ attained up to third deposition. Furthermore, the obtained composite films were powdery. This powdery film may be due to the formation of outer porous layer. In addition, the film may develop stress to cause delamination, resulting in peeling off the film after the maximum thickness **[13].**

2.2 Material characterization

The X-ray diffraction (XRD) analysis was carried out using diffractometer with chromium and copper target of wavelength 2.29 and 1.54 Å, respectively. Surface morphology is studied with the help of scanning electron microscope (SEM) model JEOL–JSM 6360. FT-IR spectroscopy was recorded between 4000-400 cm^{-1} at a spectral resolution of 2 cm^{-1} on a Perkin Elmer 1710 spectrophotometer using KBr pellets at room temperature. FT-Raman spectroscopy study is conducted using Bruker make FT-Raman spectrophotometer. Samples, in the powder form, were excited with a 514.5 nm Argon laser (0.5 mW), using a Perkin-Elmer, model 783, USA. The supercapacitive study is carried out using the 263A EG & G Princeton

Applied Research Potentiostat forming an electrochemical cell consisting of PANI-RuO_2 composite electrode as a working electrode, platinum as a counter electrode and saturated calomel electrode (SCE) as a reference electrode. The Won*A*Tech Automatic Battery Cycler, WBCS3000 system interfaced to a computer is used to study the charge-discharge of PANI-RuO_2 composite electrode. The electrochemical impedance measurement is conducted with Won*A*Tech made electrochemical workstation (ZIVE SP5).

3 Results and Discussion

3.1 PANI thin film formation and reaction mechanism

An efficient polymerization of aniline is achieved only in an acidic medium, where aniline exists as an anilinium cation. The oxidation of monomers forms a radical cations followed by coupling to form di-cations and its repetition leads to the polymer formation. The oxidation process is accompanied by the insertion of anions of acid solution in order to maintain the charge neutrality of the PANI. The oxidation of aniline with APS to yield PANI and other by products is presented in reaction 1 **[14-16],**

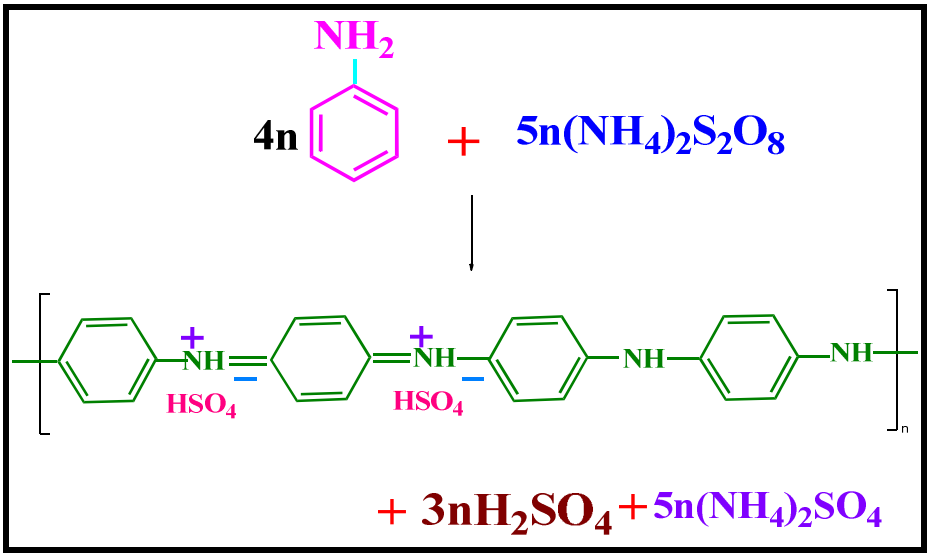

Reaction 1: Aniline is oxidized with ammonium persulfate to form PANI. Sulfuric acid and ammonium sulfate are by products.

3.2 PANI-RuO_2 composite thin film formation and reaction mechanism

The CBD is based on the formation of solid phase from a solution, which involves two steps as a nucleation and particle growth. In the nucleation, the clusters of molecules formed undergo rapid decomposition and particles combine to grow up to a certain thickness of the film by heterogeneous reactions at the substrate surface. Generally, metal ions are complexed in such a way that reaction takes place between slowly released metal ions to form product in

thin film. The APS plays the role of oxidizing agent in case of aniline monomer and provides the OH^- ions for the metal oxide.

$$(NH_4)_2S_2O_8 \rightarrow 2NH_3 + 2H^+ + S_2O_8^{2-} \quad (1)$$

In aqueous solution, ammonia releases the OH^- ions as,

$$NH_3 + H_2O \Leftrightarrow NH_4^+ + OH^- \quad (2)$$

For the deposition of RuO_2 film, $RuCl_3$ was used as a source of ruthenium ions (Ru^{3+}). The Ru^{3+} ions react with OH^- ions in the solution to form ruthenium hydroxide ($Ru(OH)_3$) which then react with excess OH^- ions to form RuO_2. The following reaction gives the formation of RuO_2,

$$2Ru(III)Cl_3 \rightarrow 2Ru^{3+} + 6Cl^- \quad (3)$$

$$Ru^{3+} + 3OH^- \rightarrow Ru(OH)_3 \quad (4)$$

$$Ru(OH)_3 + OH^- \rightarrow RuO_2 + 2H_2O \quad (5)$$

Thus, the equations 1 and 5 explained above gives the formation of PANI-RuO_2 composite thin film. The complete reaction mechanism for the formation of PANI-RuO_2 composite thin film is schematically presented in **Fig. 2.** Thickness of PANI-RuO_2 composite thin film was measured by the gravimetric weight difference method using the relation,

$$t = \Delta m / A \rho \quad (6)$$

Where, 'Δm' is the deposited weight of material, 'A' is the area and 'ρ' is the density of the material. The density of the deposited material is assumed to be same as that of the bulk material. The density of the film material is expressed as **[17],**

$$\rho = ½ (\rho_1 + \rho_2) \quad (7)$$

Where, 'ρ_1' and 'ρ_2' are bulk densities of PANI (1.30 $g.cm^{-3}$) and RuO_2 (6.97 $g.cm^{-3}$) material, respectively.

3.3 XRD study

Fig. 3 shows the XRD patterns of (a) PANI and (b) PANI-RuO_2 composite thin films onto the stainless steel substrates. The XRD patterns of PANI-RuO_2 composite **(Fig. 3 b)** thin film consists of no well-defined diffraction peaks other than stainless steel substrate, indicating the amorphous nature of PANI-RuO_2 composite thin film. Here, the stainless steel peaks position are different for PANI and PANI-RuO_2 composite thin films which is due to the different targets of Cu (λ - 1.54 Å) and Cr (λ - 2.29 Å) were used during the charecterization. Also, **Fig. 3(a)** indicates the amoprphous strucutre of PANI thin film on the stainless steel substrate. The amorphous phase obtained for each material is feasible for supercapacitor

application in this study, since the protons can easily permeate through the bulk of the amorphous material electrode and whole amount of electrode is utilized for energy storage **[18].** In this case, the material may be formed in the form nanocrystalline, but because of more intense stainless steel peaks; there may be difficulty to find out the small intensity peaks corresponding to RuO_2 or PANI thin films. But the presence of RuO_2 and PANI-RuO_2 composite material is confirmed from FT-IR and FT-Raman spectroscopy, which are more sensitive to identify to the presence of bonding or stretching vibrations in the synthesized RuO_2 and PANI-RuO_2 composite **[19].** Inset of **Fig. 3** shows the photographs of the (a) PANI and (b) PANI-RuO_2 composite thin films on the stainless steel substrate. The films are well adherent to the substrate. The PANI-RuO_2 composite films are slightly black greenish in color, different from PANI green color. Therefore, this indicates that the CBD method can be used for the deposition of PANI as well as PANI-RuO_2 composite thin films.

3.4 Surface morphological study

Fig. 4 shows the SEM images of (a) PANI and (b) PANI-RuO_2 composite thin films on stainless steel substrate at × 10,000 magnification. **Fig. 4 (a)** shows the SEM image of PANI thin film. The agglomerated and staked globular structure spread over the entire substrate surface is observed for PANI thin film. This is the agglomerated dense structure PANI particles. In addition, the PANI-RuO_2 composite shows the globular structure. It is observed from **Fig. 4 (b)** that the RuO_2 spreads a thin layer on agglomerated globular structure of PANI capturing inside RuO_2 layer. Thus, the substrate is fully covered with densely agglomerated spherical particles of PANI covered by thin layer of RuO_2 material.

3.5 FT-IR study

FT-IR spectroscopy was employed in order to identify the presence of bonding or stretching vibrations in the synthesized PANI and PANI-RuO_2 composite thin films and hence to confirm material formation. **Fig. 5** shows the FT-IR absorption spectra of (a) PANI and (b) PANI-RuO_2 composite thin films. The FT-IR spectrum of PANI-RuO_2 composite material is shown in **Fig. 5 (b).** In the spectrum, the small peaks at 608 and 502 cm^{-1} are associated with the characteristic vibrational mode of rutile RuO_2 **[20].** The peaks at 1108 and 802 cm^{-1} are attributed to the in plane and an out-of-plane C-H bending mode, respectively. The peak at 1301 cm^{-1} corresponds to N-H bending **[21]**. The peaks at 1582 and 1477cm^{-1} are assigned to C-C ring stretching vibrations. The peak at 2931 cm^{-1} is assigned to the free N-H stretching vibrations of secondary amines and vibration associated with the NH^{2+} part in the $-C_6H_4NH^{2+}C_6H_4-$ group **[22].** The characteristic peak N-H stretching of PANI **(Fig.5 (a))** disappeared in the PANI-RuO_2 composite thin films. Along with this, the characteristic PANI

peaks at 2901, 1603, 1461 and 1110 cm^{-1} are changed to 2931, 1582, 1477 and 1108 cm^{-1}, respectively. This may be due to the strong interaction of ruthenium particles and N-H stretching group in the PANI. This result indicates the formation of PANI-RuO_2 composite thin film **[23]**.

3.6 FT-Raman study

In order to get insight about the bending and stretching vibrations, the films are characterized for their FT-Raman spectra. **Fig. 6** shows the FT-Raman spectra of (a) PANI and (b) PANI-RuO_2 composite thin films. **Fig. 6 (b)** shows FT-Raman spectrum of PANI-RuO_2 composite. In the Raman spectrum of PANI-RuO_2, the peaks at 521 and 720 cm^{-1} correspond to the crystalline ruthenium oxide in the rutile form **[24, 25]**. The bands at 1175 and 1505 cm^{-1} are assigned mainly to the benzenoid C-C ring stretching vibrations and a band at 1591 cm^{-1} is attributed to the quinoid C=C stretching mode of the polymer chain **[26]**. The characteristic band 1367 cm^{-1} corresponds to C=N stretching of quinoid units **[27].** In Fig. 6 (a) the peaks at 1172, 1373, 1508 cm^{-1} and 1594 cm^{-1} corresponds to the amorphous PANI **[28].** It is observed that, some characteristics peaks of PANI have been shifted in PANI-RuO_2 spectrum. The shifting of the peaks in PANI-RuO_2 spectrum may be due to the interaction of PANI chain and RuO_2 particles. Thus, the FT-Raman indicates the formation of PANI-RuO_2 composite material.

3.7 Cyclic voltammetry

The performance of PANI-RuO_2 composite as an electrode material for supercapacitor is investigated by cyclic voltammetry (CV) technique. **Fig. 7** shows the cyclic voltammograms of the (a) PANI and (b) PANI-RuO_2 composite thin film electrode at 5 $mV.s^{-1}$ scan rate. The shapes of the CV curves of PANI and PANI-RuO_2 composite are fewer rectangular within the measured potential window of -0.2 to + 0.8 V vs. SCE in 1 M H_2SO_4 electrolyte. It is observed that the CV curve for the composite reveals redox peaks with enhanced current background than the PANI electrode. Two pairs of redox peaks corresponding to leucoemeraldine to emeraldine salt conversion (first pair P1 and P4) and emeraldine salt to pernigraniline conversion of PANI are clearly observed (second pair P2 and P3) **[29, 30]**. The CV curve reveals a redox behavior of PANI-RuO_2 composite electrode different from electrical double layer capacitance. The specific capacitances of PANI and PANI-RuO_2 composite electrode are found to be 591 and 830 $F.g^{-1}$, respectively at the scan rate of 5 $mV.s^{-1}$. The PANI-RuO_2 composite electrode shows enhanced specific capacitance than the pristine PANI electrode. Composites of PANI with RuO_2 are promising because PANI acts an excellent material to host the active RuO_2 sites in this case. Also, intense improvements in their properties and performances due to the synergistic effect between the two ingredients and this may be because

of RuO_2 served as an intercalated spacer to further enhance the host surface area **[6, 31].** Zhang et al. reported the enhanced specific capacitance of PANI-MnO_2 composite due to synergistic effect **[29]**.

3.8 Effect of scan rate

The voltammetric responses of PANI-RuO_2 composite electrode at different scan rates are shown in **Fig. 8**. It is found that the current under curve is slowly increased with scan rate. This shows that a voltammetric current is directly proportional to the scan rate of CV, indicating pseudocapacitive behavior **[32]**. The cyclic voltammograms at high scan rates do not show redox peaks over the potential range, due to the slow kinetics of the surface redox reaction of the electrode as well as the limited proton diffusion migration than at the low scan rate **[33]. Fig. 9** shows the variation of specific capacitance of (a) PANI and (b) PANI-RuO_2 composite electrodes, respectively. The specific capacitance is decreased from 830 to 255 Fg^{-1} as the scan rate increased from 5 to 100 mVs^{-1}. The maximum specific capacitance of 830 Fg^{-1} is obtained for PANI-RuO_2 composite thin film electrode at lower scan rate of 5 mVs^{-1}. Patil et al. obtained a maximum specific capacitance of 73 Fg^{-1} for $RuO_2.H_2O$ on the stainless steel substrate by CBD method **[34].** Hu et al. reported a maximum specific capacitance of 100 Fg^{-1} for $RuO_2.H_2O$ electroplated on to a titanium substrate by CV from an aqueous solution **[35].** The comparative studies with other reports have been made in **Table 1.** The specific capacitance of the PANI-RuO_2 composite synthesized by CBD method is comparable and higher than the PANI-RuO_2 composites made by other methods **(Table 1).** It is observed that the specific capacitance obtained in the present work is than the other reported work **[9, 36-38].**

Fig. 10 shows the variation of interfacial capacitance of (a) PANI and (b) PANI-RuO_2 composite thin film electrodes, respectively. The interfacial capacitance is decreased from 0.099 to 0.03 Fcm^{-2} as the scan rate increased from 5 to 100 mVs^{-1}. From the **Figs. 9 and 10**, it is observed that the specific and interfacial capacitances of PANI and PANI-RuO_2 composite thin film electrode decreased with the increased scan rates. Here, the decrease in capacitance values with the scan rate are attributed to the presence of inner active sites, which cannot precede the redox transitions completely at higher scan rate of CV, probably due to the diffusion effect of proton within the electrode **[39].** In addition, it has been attributed to the resistance of ion diffusion, which becomes significant under relatively high scan rate as well as the proportion of inaccessible sites increases with increase in scan rate of CV, therefore a decrease in the specific capacitance is observed accordingly **[40]**.

3.9 Stability study

Long cycle life is a crucial parameter for supercapacitor electrode materials. Stability of PANI-RuO_2 composite electrode is tested by CV. **Fig. 11** shows the specific capacitance as a function of cycle number of (a) PANI and (b) PANI-RuO_2 composite electrodes. It is observed that the PANI-RuO_2 composite electrode shows the 85% stability over the 5000^{th} CV cycles. The pristine PANI electrode shows the 70% stability over the same CV cycles. Since a thin layer of RuO_2 is spread over the PANI during the deposition, which can provide shield to volume change of PANI during stability, because of counter ions intercalation/deintercalation. In addition, this may prevent the breakage of PANI chain during the charging and discharging process resulting the enhanced stability **[31]**. Inset of **Fig. 11** shows the CV curves of PANI-RuO_2 composite electrode for the 1^{st} and 5000^{th} cycles at the scan rate of 100 mVs^{-1}. The specific capacitance for the 1^{st} cycle is 255 Fg^{-1} and it is decreased upto 217 Fg^{-1} for 5000^{th} cycle. The current under curve is decreased by 15% up to 5000^{th} cycles. The small amount of decrease in specific capacitance of PANI-RuO_2 composite electrode value is observed due to the loss of active material with the cycle number. Hence, it illustrates the stable nature of PANI-RuO_2 composite electrode in energy storage application.

3.10 Charge-discharge study

The galvanostatic charge-discharge is a consistent method to assess the electrochemical capacitance of materials under precise current conditions. The charge–discharge behavior of the (a) PANI and (b) PANI-RuO_2 composite thin film electrodes is shown in **Fig. 12**. The charge-discharge study is carried out at 0.5 $mAcm^{-2}$ current density in the potential range of -0.2 to 0.8 V vs. SCE. In the charge-discharge curves of (a) PANI, and (b) PANI-RuO_2 composite thin film electrodes, the charging curves are not exactly symmetric with discharging curve i.e. perfect linear curves are not obtained compared with EDLC. This indicates a typical pseudocapacitance behavior resulting from the electrochemical adsorption/absorption or redox reactions at interfaces between electrodes and electrolyte. When the potential is reversed, the total impedance of the cell gave rise to a large initial IR drop (potential drop) during discharge process, which remained until the constant capacitive performances have been achieved. The large IR drop is due to the higher internal resistance of the electrode materials, which implies that the electrode materials lack electrochemical reversibility and capacitive characteristics. At low potential, discharge response of the capacitor approached an ideal linear charge-discharge voltage relationship **[41, 42].** The potential drop for PANI-RuO_2 composite electrode is less as compared to the PANI electrode. This result reflects that the internal resistance of PANI-RuO_2 composite is smaller than the PANI. Low internal resistance is of great importance in energy

storage devices, as the less energy would be wasted to produce unwanted heat during the charging–discharging processes **[43].** The different parameters of supercapacitors, such as specific power, specific energy and columbic efficiency are evaluated from the charge-discharge curves of the PANI and PANI-RuO_2 composite thin film electrode. The specific power (SP) and specific energy (SE) are calculated using the following relations **[44],**

$$SP = [I \times V] / m \quad (8)$$

$$SE = [I \times t \times V] / m \quad (9)$$

Where, SP is specific power in $KWkg^{-1}$ and SE is specific energy in $Whkg^{-1}$. The above expressions shows the discharge current (I) in amperes, voltage range (V) in volts, discharge time (t) in seconds and mass of the electroactive material (m) in kilograms. The coulombic efficiency is calculated using the following equation **[45],**

$$\eta = [t_D / t_C] \times 100 \quad (10)$$

Where, t_C and t_D represent the charging and discharging time, respectively. The specific power, specific energy and columbic efficiency estimated from the charge-discharge curves are given in the **Table 2.** It is observed that the supercapacitor parameters of PANI-RuO_2 composite electrode are larger than the PANI electrode showing more suitability of composite for the supercapacitor application.

3.11 Electrochemical impedance spectroscopy (EIS) study

The typical Nyquist plots between real (Z') and imaginary (Z") parts of impedance data of (a) PANI and (b) PANI-RuO_2 composite electrodes are shown in **Fig. 13**. The PANI-RuO_2 composite thin film shows semicircle in the high frequency region and in the low frequency region the linear region leans more toward the imaginary axis (shows the vertical line) and this indicates good capacitive behavior **[46]**. PANI thin film shows the semicircle in the high frequency region and nearly vertical line in the low frequency region similar to PANI-RuO_2 composite electrode. Inset of **Fig. 13** shows enlarged view of semicircles of electrodes. From the EIS study, it observed that the charge transfer resistance for the PANI-RuO_2 composite electrode (9 Ω) is smaller than the electrochemical series resistance (ESR) of PANI (20 Ω) electrode.

4. Conclusions

A simple CBD method has been used to prepare PANI-RuO_2 composite thin film electrodes for supercapacitor application. The SEM images show the spherical clusters of PANI encapsulated under thin layer of RuO_2 in the PANI-RuO_2 composite. There is a strong interaction between RuO_2 particle and PANI chain, since the shifting and decrease in relative

intensity of bands are observed in the FT-IR and FT-Raman study. This confirms the formation of PANI-RuO_2 composite material. The PANI-RuO_2 composite electrode exhibits a maximum specific capacitance of 830 Fg^{-1}. It shows good cycling performance and keeps 85% of initial capacity over 5000^{th} cycles. The electrochemical impedance study reveals the supercapacitive behavior. From the comparative study of PANI and PANI-RuO_2 composite supercapacitor, it is observed that formation of composite material enhance supercapacitive performance of pristine material. These results suggest that the PANI–RuO_2 composite can be used for supercapacitor application.

Acknowledgment

Authors are grateful to UGC and DST New Delhi for providing finance through the UGC-DSA-Phase-I, DST-PURSE and DST-FIST programme to the department of physics.

References

[1] V. Etacheri, R. Marom, R. Elazari, G. Salitra and D. Aurbach, Energy Environ. Sci., 2011, **4**, 3243-3262.

[2] A. Balducci, R. Dugas, P. Taberna, P. Simon, D. Plee, M. Mastragostino and S. Passerini, J. Power Sources, 2007, **165**, 922-927.

[3] C. G. Liu, Z. N. Yu, D. Neff, A. Zhamu and B. Z. Jang, Nano Lett., 2010, **10**, 4863-4871.

[4] D. W. Wang, F. Li, Z. G. Chen, G. Q. Lu, and H. M. Cheng, Chem. Mater. 2008, **20,** 7195–7200

[5] G. Lota, K. Fic, and E. Frackowiak, Energy Environ. Sci., 2011, **4**, 1592-1605.

[6] N. A. Kumar and J. B. Baek, Chem. Commun., 2014, **50**, 6298-6308.

[7] X. X. Liu, L.J. Bian, L. Zhang, and L. J. Zhang, J. Solid State Electrochem., 2007, **11**, 1279-1286.

[8] S. M. Lin, and T. C. Wen, Electrochim. Acta, 1994, **39**, 393-400.

[9] S. Sopcic, M. K. Rokovic, Z. Mandic, and G. Inzelt, J. Solid State Electrochem., 2010, **14,** 2021-2026.

[10] S. F. Shaikh, J. Y. Lim, and O. S. Joo, Curr. Appl. Phy. **2013,** 13, 758-761.

[11] P. R. Deshmukh, N. M. Shinde, S. V. Patil, R. N. Bulakhe, and C.D. Lokhande, Chem. Engg. J., 2013, **223,** 572–577.

[12] P. R. Deshmukh, S. N. Pusawale, A. D. Jagadale, and C. D. Lokhande, J. Mater. Science, 2012, **47**, 1546-1553.

[13] U. M. Patil, K. V. Gurav, O. S. Joo, and C. D. Lokhande, J. Alloys Comp., 2009, **478,**

711-715.

[14] J. Huang, and R. B. Kaner, Chem. Commun., 2006, 367–376.

[15] J. Stejskal, I. Sapurina, M. Trchova, E. N. Konyushenko, and P. Holler, Polymer, 2006, **47,** 8253-8262.

[16] H. D. Tran, J. M. D'Arcy, Y. Wang, P. J. Beltramo, V. A. Strong, and R. B. Kaner, J. Mater. Chem., 2011, **21,** 3534–3550.

[17] B. R. Sankpal, and C. D. Lokhande, Mater. Chem. Phy., 2002, **74**, 126-133.

[18] V. D. Patake, and C. D. Lokhande, Appl. Surf. Sci., 2008, **254,** 2820-2824.

[19] M. Grzeszczuk, A. Granska, and R. Szostak, Int. J. Electrochem. Sci., 2013, **8,** 8951-8965

[20] J. Mink, J. Kristof, A. D. Battisti, S. Daalio, and C. Nemeth, Surf. Sci., 1995, **335,** 252-257.

[21] P. S. Rao, J. Anand, S. Palaniappan, and D. N. Sathyanarayana, European Polym. J., 2000, **36,** 915-921.

[22] S. B. Kulkarni, S. S. Joshi, and C. D. Lokhande, Chem. Eng. J., 2011, **166,** 1179-1185.

[23] C. R. K. Rao, and M. Vijayan, Synth. Met., 2008, **158,** 516-519.

[24] J. Haines, J. M. Leger, M. W. Schimidt, J. P. Petitet, A. S. Pereira, J. A. H. da Jornada, and S. Hull, J. Phys. Chem. Solids, 1998, **59,** 239-242.

[25] J. Y. Kim, K. H. Kim, S. H. Park, and K. B. Kim, Electrochim. Acta, 2012, **55**, 8056-8061.

[26] Z. Ping, G. E. Nauer, H. Neugabauer, J. Theiner, and A. Neckel, J. Chem. Soc., Faraday Trans., 1997, **93**, 121-129.

[27] M. Sacak, U. Akbulut, and D. N. Batchelder, Polym., 1998, **40,** 21-26.

[28] S. Sinha, S. Bhadra, and D. Khastgir, J. Appl. Polym. Sci., 2009, **112,** 3135-3140.

[29] X. Zhang, L. Ji, S. Zhang, and W. Yang, J. Power Sources, 2007, **173,** 1017-1023.

[30] M. Kaneko, and K. Kaneto, Polymer, 2001, **33,** 104-107.

[31] Z. Tong, Y. Yang, J. Wang, J. Zhao, B. L. Suc and Y. Li, J. Mater. Chem. A, 2014, **2**, 4642-4651.

[32] J. N. Broughton, and M. J. Brett, Electrochem. Solid State Lett., 2002, **5**, A279-A282.

[33] J. H. Park, S. H. Kim, J. M. Ko, Y. G. Lee, and K. M. Kim, J. Electrochem. Sci. Technol., 2011, **2,** 211-215.

[34] U. M. Patil, S. B. Kulkarni, V. S. Jamadade, and C. D. Lokhande, J. Alloys Comp., 2011, **509,** 1677-1682.

[35] C. C. Hu, and Y. H. Huang, J. Electrochem. Soc., 1999, **146,** 2465-2471.

[36] H. S. Nam, K. M. Kim, S. H. Kim, B. C. Kim, G. G. Wallace, J. M. Ko, Polym. Bull., 2012, **68,** 553-560.

[37] X. Li, W. Gan, F. Zheng, L. Li, N. Zhu, X. Huang, Synth. Met., **162**, 2012, 953–957.

[38] P. R. Deshmukh, S. V. Patil, R. N. Bulakhe, S. D. Sartale, C. D. Lokhande, Chem. Engg. J., 2014, **257,** 82–89.

[39] J. J. Zhu, Z. H. Lu, S. T. Aruna, D. Aurbach, and A. Gednken, Chem. Mater., 2000, **12,** 2557-2566.

[40] S. Mitali, D. Soma, and D. Monica, Res. J. Chem. Sci., 2011, **1,** 109-113.

[41] J. J. Cai, L. B. Kong, J. Zhang, Y. C. Luo, L. Kang, Chinese Chemical Letters, 2010, **21** 1509–1512.

[42] P. R. Deshmukh, S. N. Pusawale, V. S. Jamadade, U. M. Patil, C. D. Lokhande, J. Alloys. Comp., 2011, **509,** 5064–5069.

[43] X. Xia, Q. Hao, W. Lei, W. Wang, D. Sun, and X. Wang, J. Mater. Chem., 2012, **22,** 16844-16850.

[44] R. K. Prasad, and N. Munichandraiah, Electrochem. Solid State Lett., 2002, **5**, A271-A274.

[45] V. Ganesh, S. Pitchumani, and V. Lakshminarayanan, J. Power Sources, 2006, **158,** 1523-1532.

[46] L. Mao, K. Zhang, H. Sze On Chan and J. Wu, J. Mater. Chem., 2012, **22**, 80-85.

Figure captions

Fig. 1: The schematic illustration of CBD method for the deposition of PANI-RuO_2 composite thin films.

Fig. 2: Growth mechanism for the PANI-RuO_2 composite thin film.

Fig. 3: XRD patterns of (a) PANI, and (b) PANI-RuO_2 composite thin films on stainless steel substrate. Inset shows the photographs of the (a) PANI, and (b) PANI-RuO_2 composite thin films deposited on the stainless steel substrate.

Fig. 4: SEM micrographs of (a) PANI, and (b) PANI-RuO_2 composite thin film on stainless steel substrate at x 10,000 magnification.

Fig. 5: FT-IR spectra of (a) PANI, and (b) PANI-RuO_2 composite thin films.

Fig. 6: FT-Raman spectra of (a) PANI, and (b) PANI-RuO_2 composite thin films.

Fig.7: CV curves of (a) PANI, and (b) PANI-RuO_2 composite thin film electrodes.

Fig. 8: CV curves of PANI-RuO_2 composite thin film electrodes at various scan rates.

Fig. 9: The effect of scan rate on specific capacitance of (a) PANI, and (b) PANI-RuO_2 composite thin film electrodes.

Fig.10: The effect of scan rate on interfacial capacitance of (a) PANI, and (b) PANI-RuO_2 composite thin film electrodes.

Fig.11: Variation of specific capacitance of (a) PANI, and (b) PANI-RuO_2 composite thin film electrode with cycle number. Inset of Fig. 11 shows CV curves of PANI-RuO_2 composite electrode at 1^{st} and 5000^{th} cycles at the scan rate of 100 mVs^{-1}.

Fig.12: Galvanostatic charge-discharge curves of (a) PANI, and (b) PANI-RuO_2 composite thin film electrodes.

Fig.13: Nyquist plots of (a) PANI, and (b) PANI-RuO_2 composite thin film electrodes [Inset of Fig.13 shows the enlarge view of Nyquist plots].

Figures

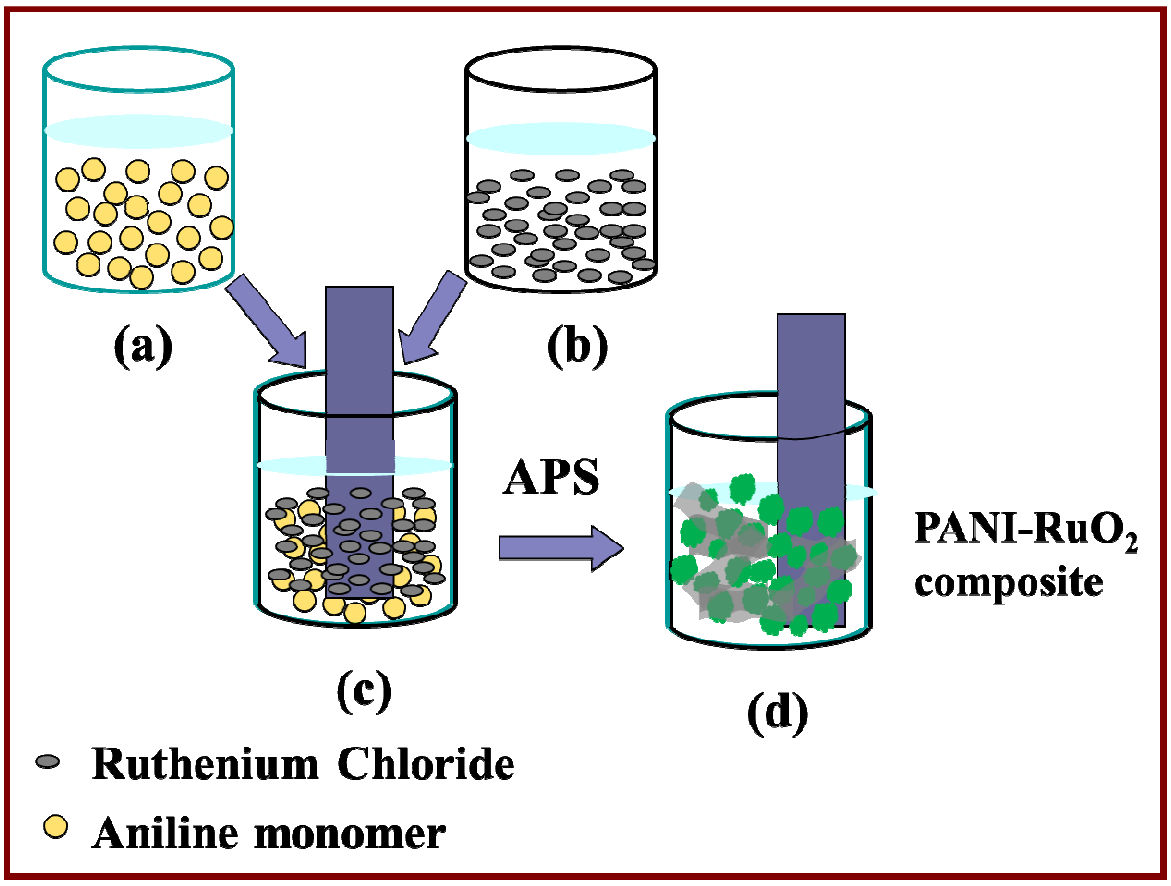

Fig. 1

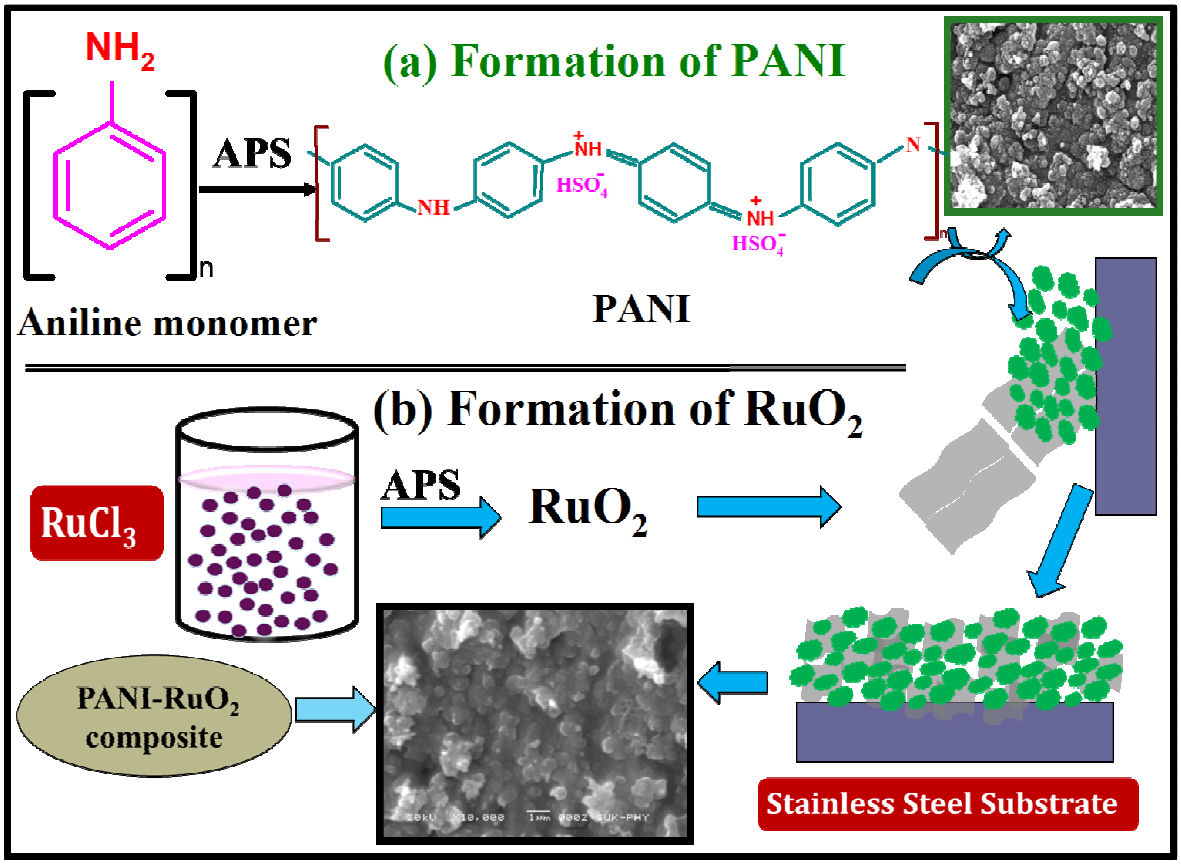
NH2
(a) Formation of PANI
APS
NH
HSO4
N
n
Aniline monomer
PANI
(b) Formation of RuO2
RuCl3
APS
RuO2
PANI-RuO2 composite
Stainless Steel Substrate

Fig. 2

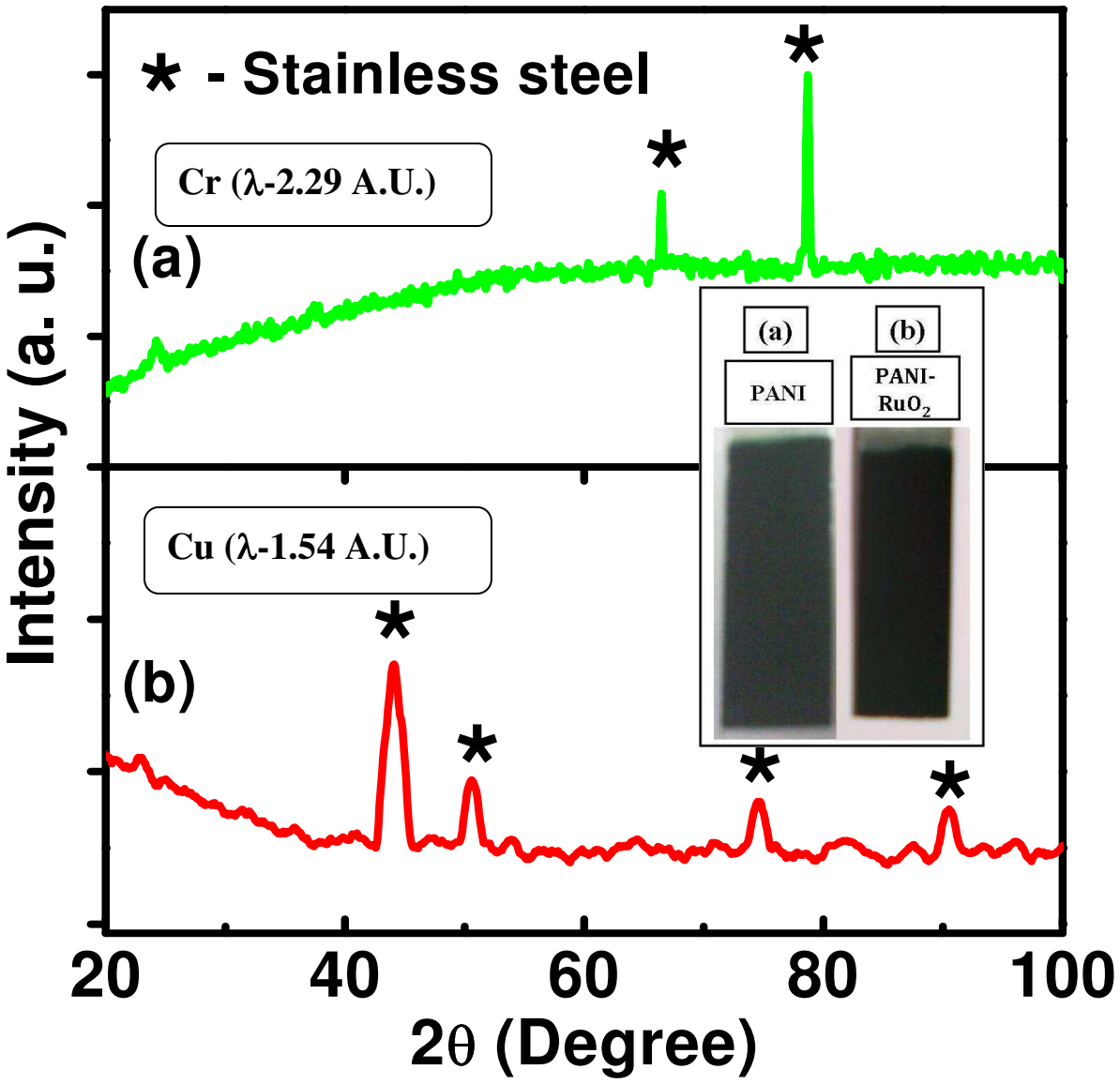
* - Stainless steel
Cr (λ-2.29 A.U.)
(a)
Cu (λ-1.54 A.U.)
(b)
(a)
(b)
PANI
PANI-RuO2
Intensity (a. u.)
20
40
60
80
100
2θ (Degree)

Fig. 3

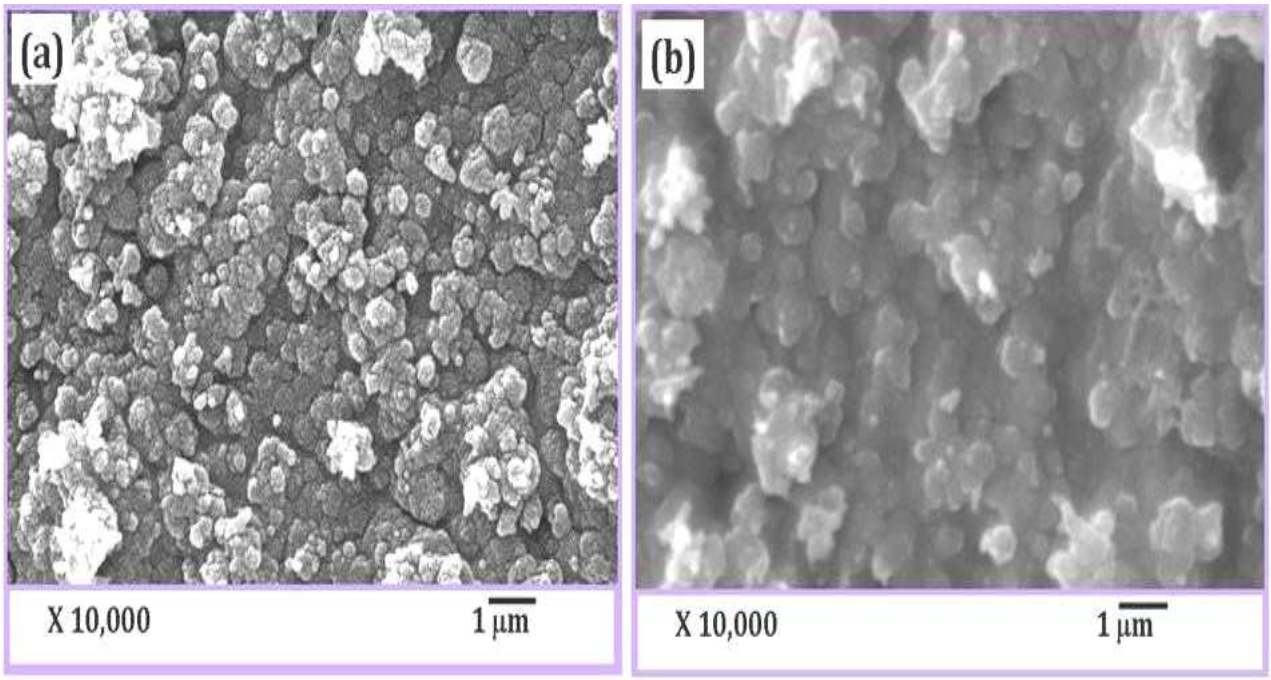

Fig. 4

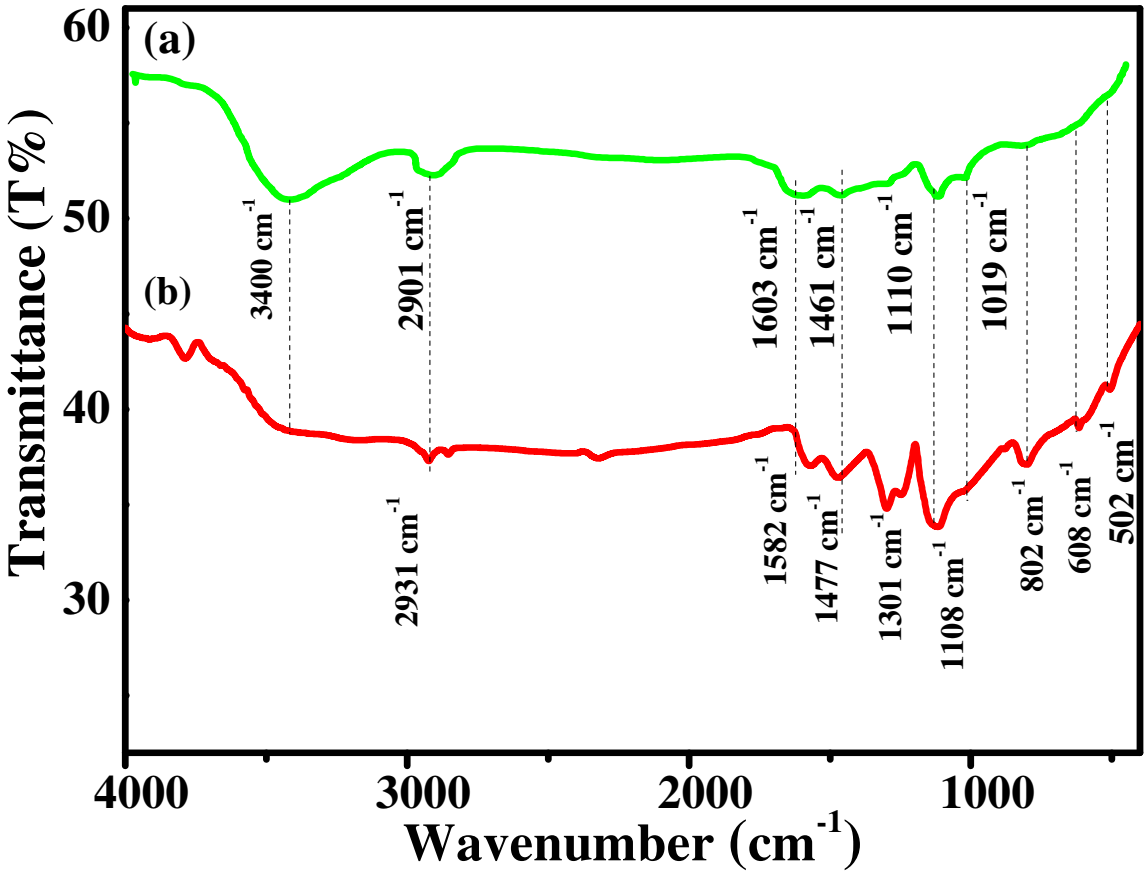
(a)
(b)
Transmittance (T%)
60
50
40
30
4000
3000
2000
1000
Wavenumber (cm-1)
3400 cm-1
2901 cm-1
1603 cm-1
1461 cm-1
1110 cm-1
1019 cm-1
2931 cm-1
1582 cm-1
1477 cm-1
1301 cm-1
1108 cm-1
802 cm-1
608 cm-1
502 cm-1

Fig. 5

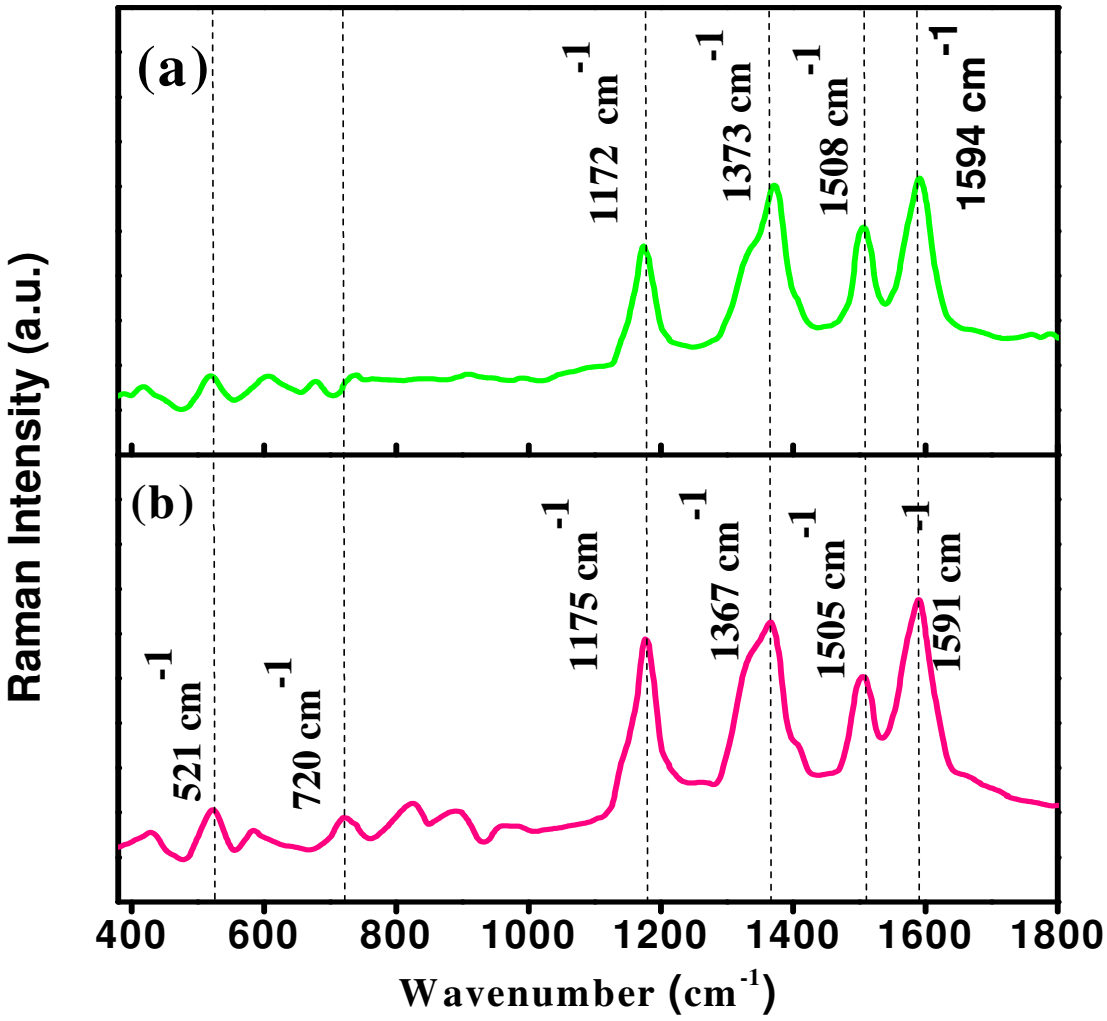
(a)
1172 cm-1
1373 cm-1
1508 cm-1
1594 cm-1
(b)
521 cm-1
720 cm-1
1175 cm-1
1367 cm-1
1505 cm-1
1591 cm-1
Raman Intensity (a.u.)
400
600
800
1000
1200
1400
1600
1800
Wavenumber (cm-1)

Fig. 6

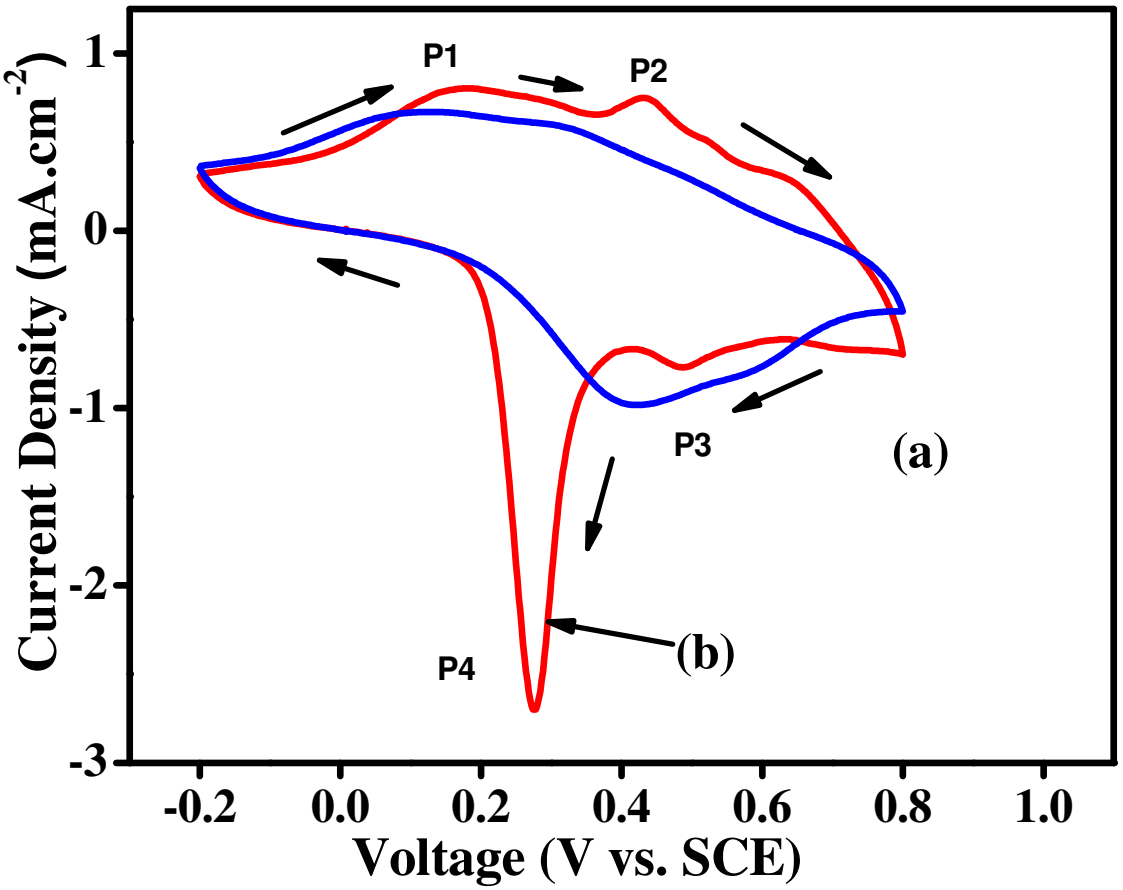
P1
P2
P3
P4
(a)
(b)
Current Density (mA.cm-2)
Voltage (V vs. SCE)
1
0
-1
-2
-3
-0.2
0.0
0.2
0.4
0.6
0.8
1.0

Fig. 7

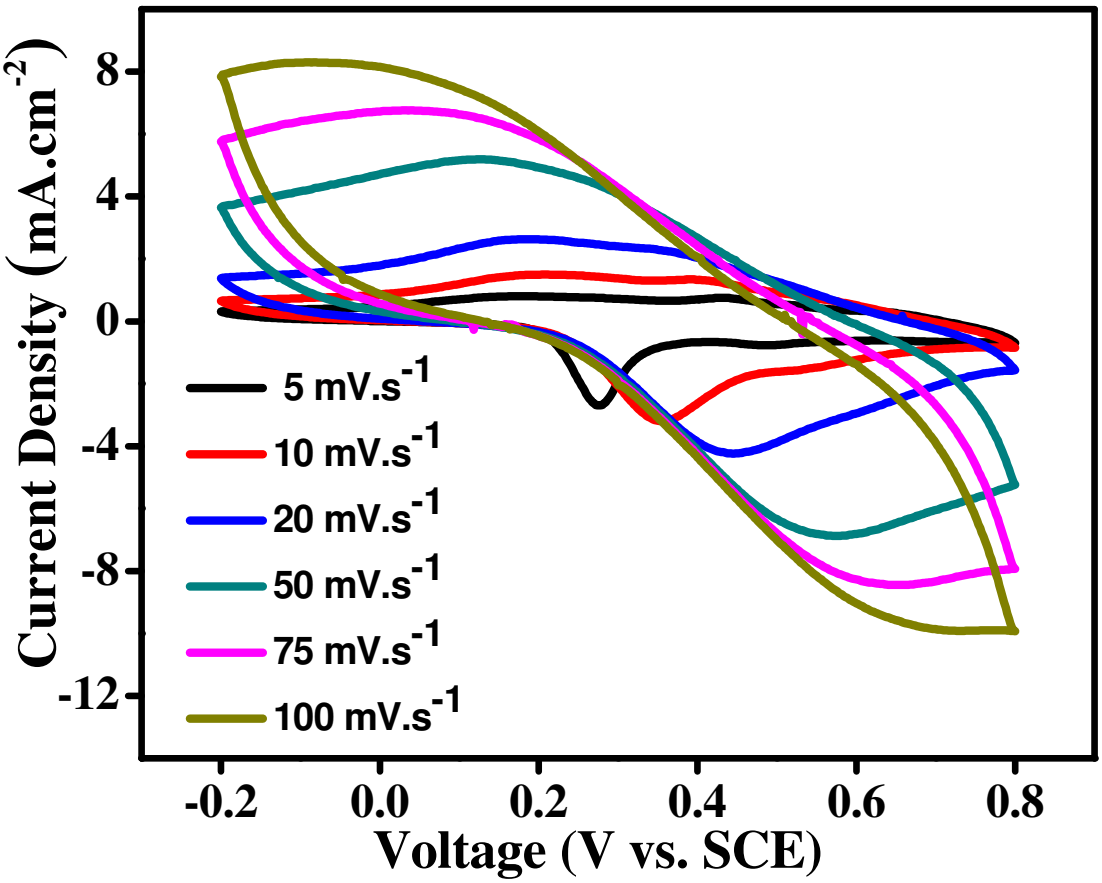
Current Density (mA.cm-2)
8
4
0
-4
-8
-12
-0.2
0.0
0.2
0.4
0.6
0.8
Voltage (V vs. SCE)
5 mV.s-1
10 mV.s-1
20 mV.s-1
50 mV.s-1
75 mV.s-1
100 mV.s-1

Fig. 8

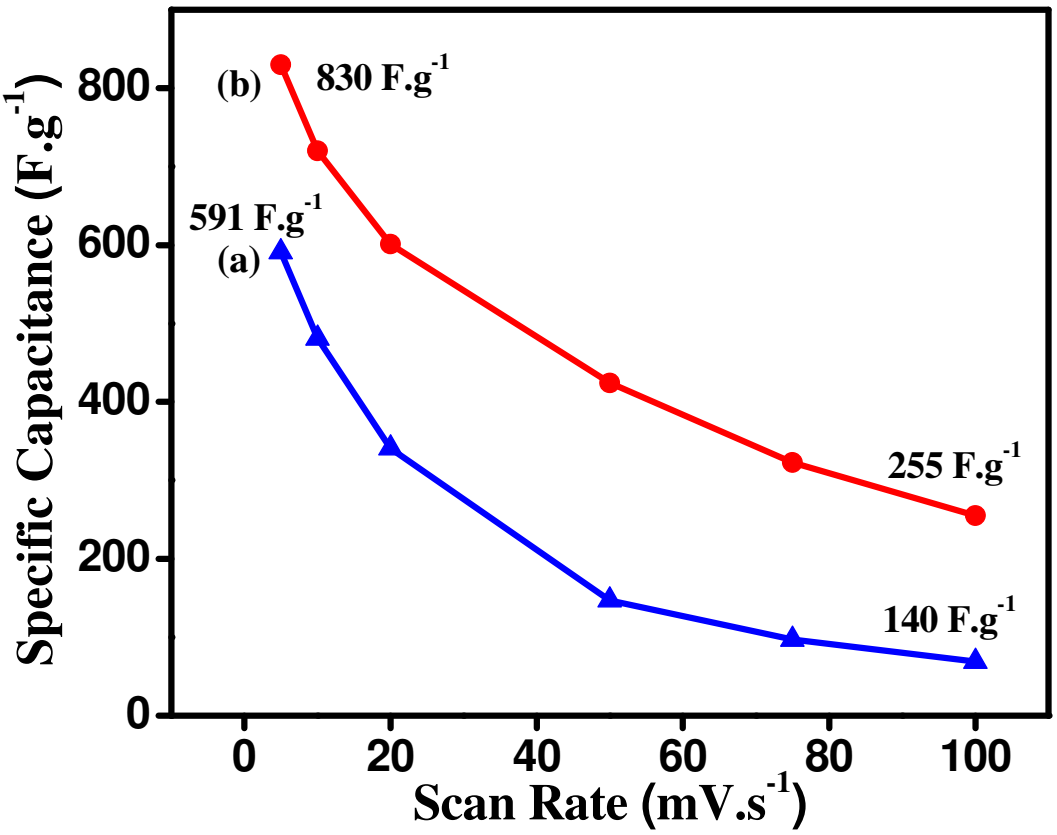
Specific Capacitance (F.g-1)
Scan Rate (mV.s-1)
(b)
830 F.g-1
591 F.g-1
(a)
255 F.g-1
140 F.g-1
0
200
400
600
800
0
20
40
60
80
100

Fig. 9

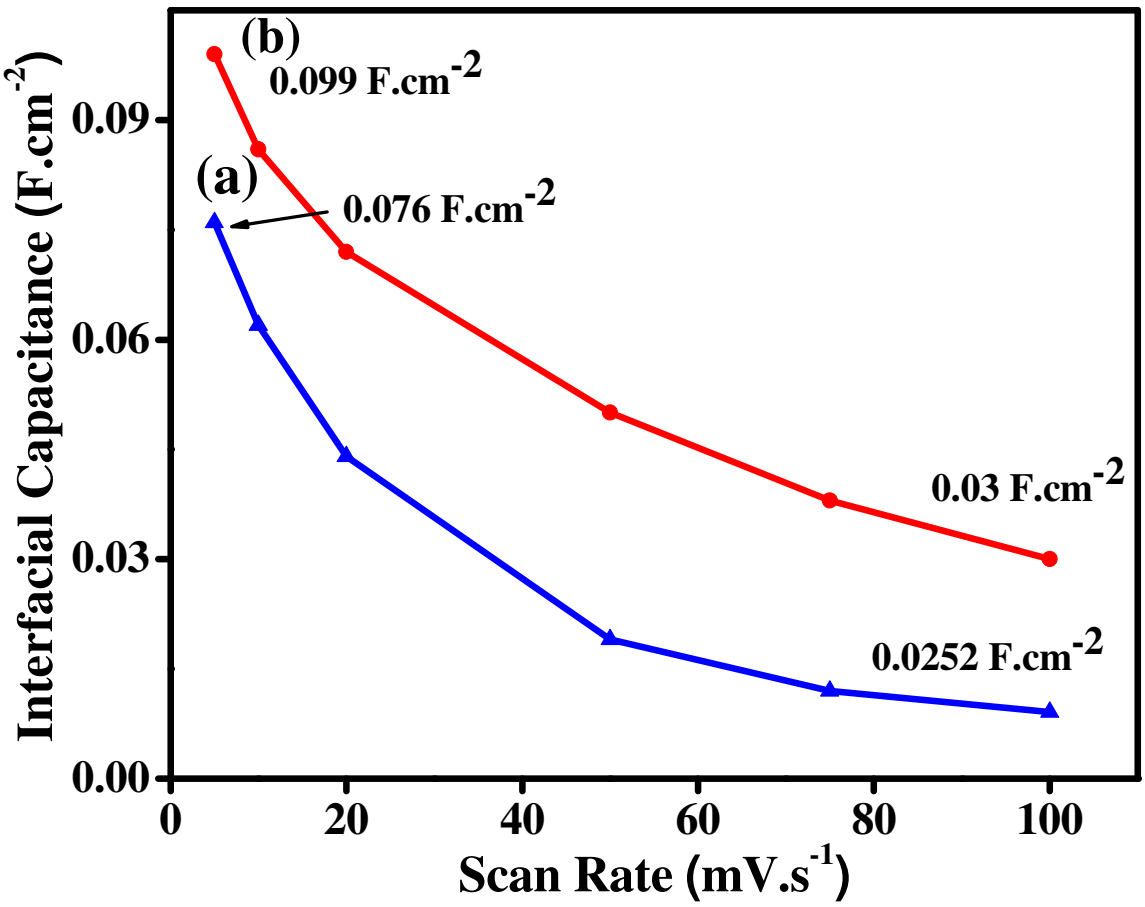
(b)
0.099 F.cm-2
(a)
0.076 F.cm-2
0.03 F.cm-2
0.0252 F.cm-2
Interfacial Capacitance (F.cm-2)
Scan Rate (mV.s-1)
0.00
0.03
0.06
0.09
0
20
40
60
80
100

Fig. 10

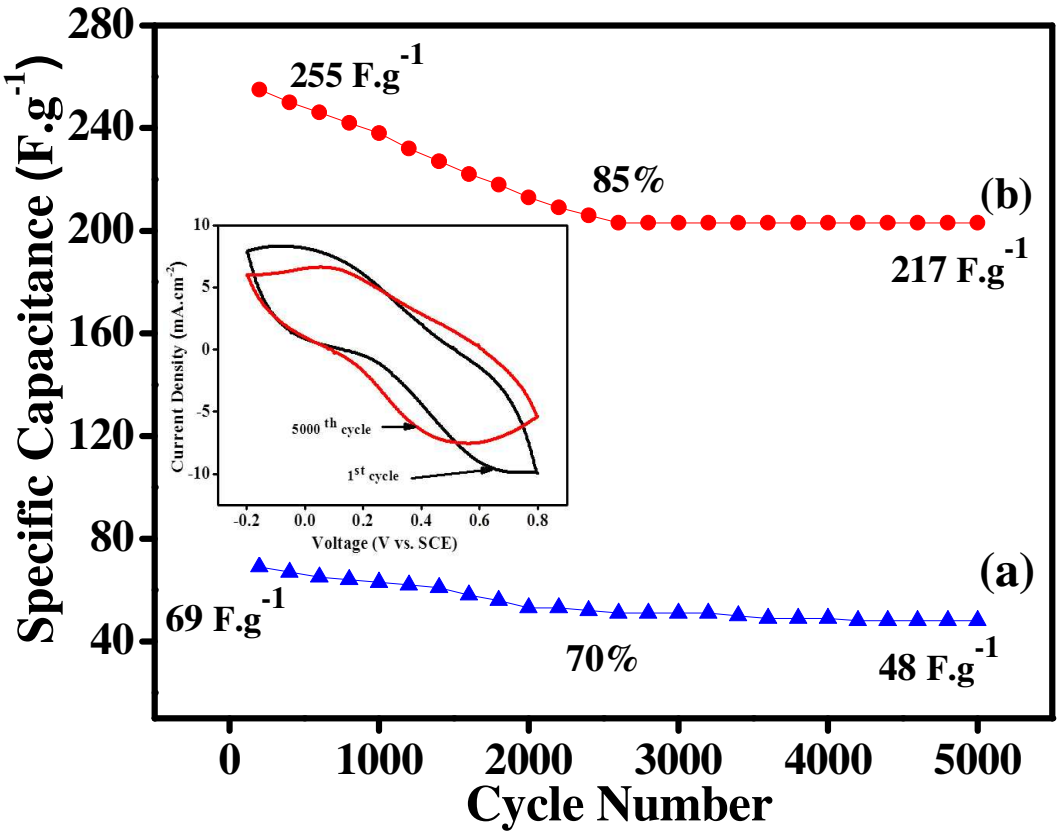
Specific Capacitance (F.g-1)
Cycle Number
255 F.g-1
85%
(b)
217 F.g-1
69 F.g-1
70%
(a)
48 F.g-1
Current Density (mA.cm-2)
Voltage (V vs. SCE)
5000 th cycle
1st cycle

Fig. 11

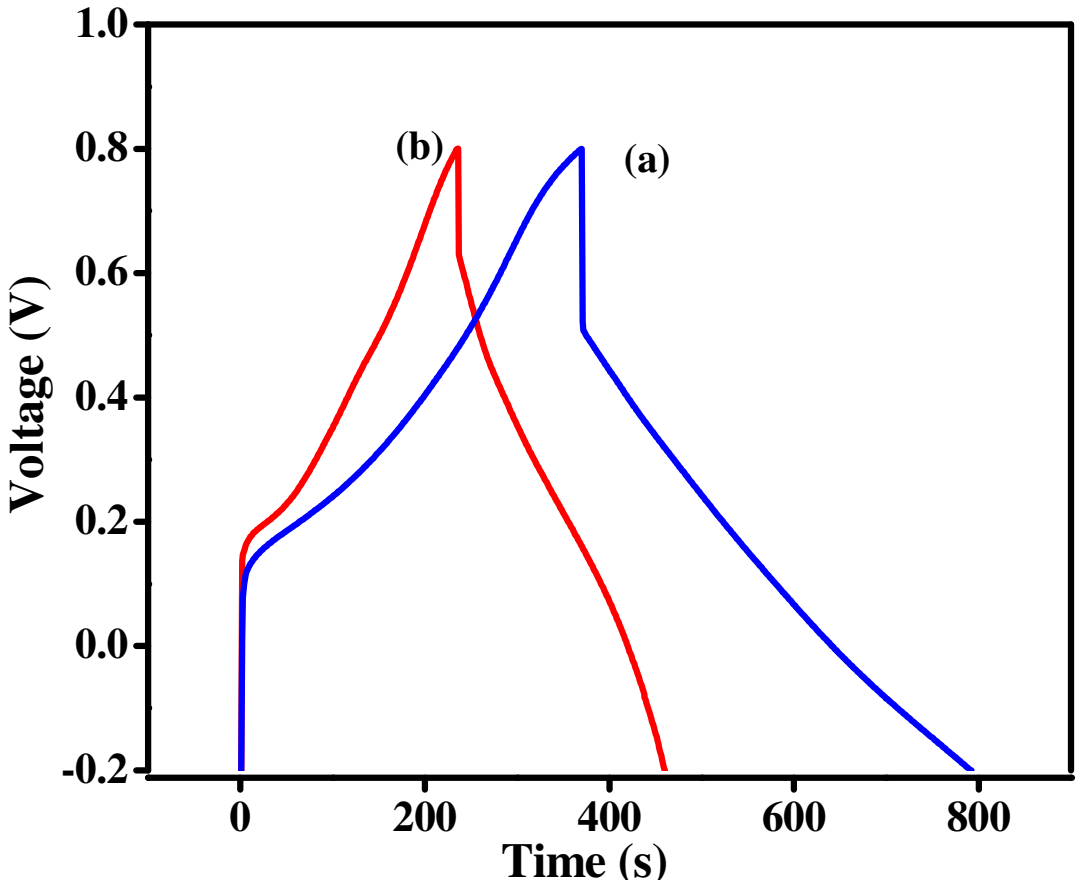

Fig. 12

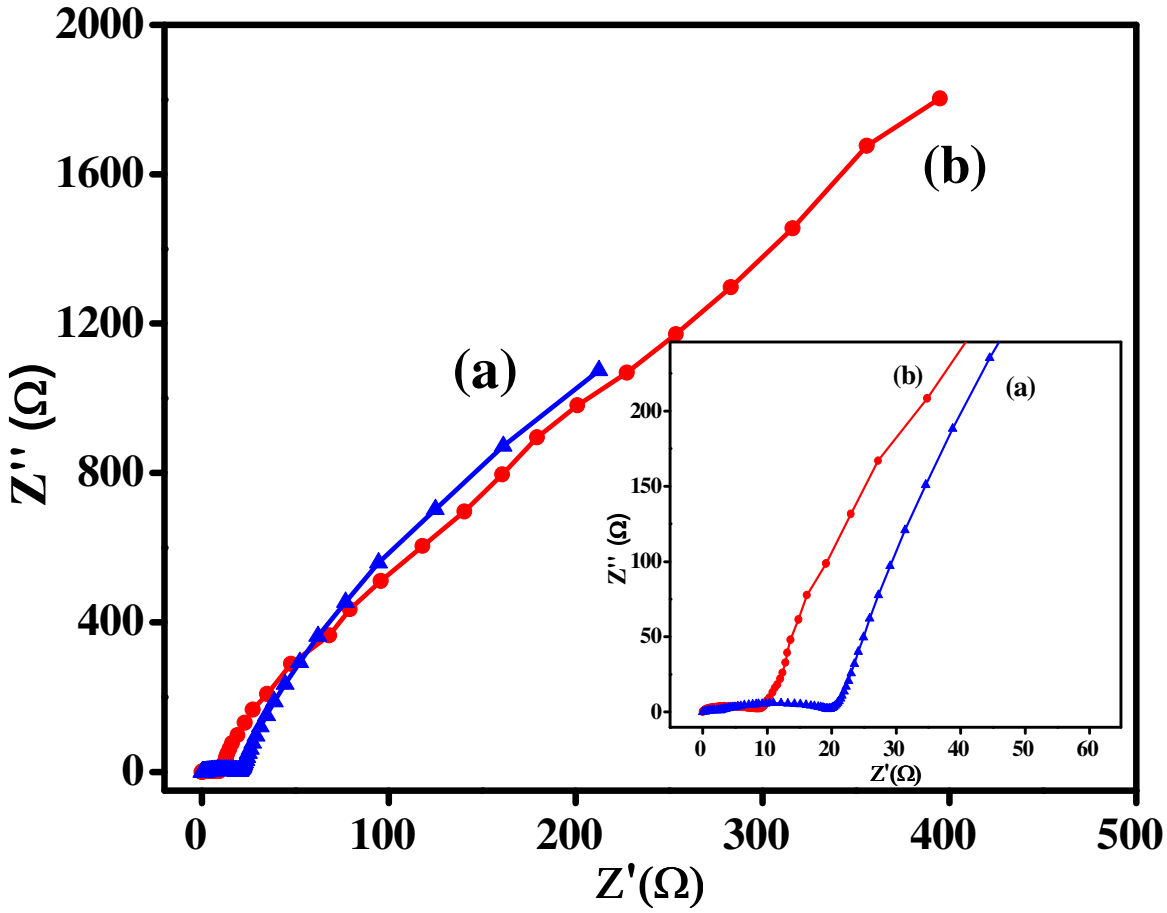
2000
1600
1200
800
400
0
Z'' (Ω)
0
100
200
300
400
500
Z'(Ω)
(a)
(b)
200
150
100
50
0
Z'' (Ω)
0
10
20
30
40
50
60
Z'(Ω)
(b)
(a)

Fig. 13

Table 1

Sr. No.	Material/ (Method)	Electrolyte	PW Volt	Scan Rate $mV.S^{-1}$	Cell Type	Active Mass	Cs $F.g^{-1}$	Ref.
1	PANI-RuO_2 (ED)	0.5 M H_2SO_4	0 to 1	50	3-Electrode	-	322	10
2	PANI- RuO_2 (ED and precipitation)	1 M H_2SO_4	0 to 1	5	3-Electrode	0.09 g	708	36
3	PANI-RuO_2 (ED)	0.5 M H_2SO_4	-0.6 to 0.6	10	3-Electrode	-	605	37
4	PANI-RuO_2 (SILAR)	1 M H_2SO_4	0 to 1	5	3-Electrode	0.14 mg/cm^2	664	38
5	PANI-RuO_2 (CBD Method)	1 M H_2SO_4	0 to 1	5	3-Electrode	0.12 mg/cm^2	830	Present Work

ED = Electrodeposition, CBD= Chemical Bath Deposition, PW=Potential Window

Cs = Specific Capacitance, Ref. = Reference.

Table 2

Supercapacitive parameters of PANI and PANI-RuO_2 composite electrodes.		
Parameters/ Material	PANI-RuO_2	PANI
Specific Power (S.P.) $kWkg^{-1}$	4.16	3.84
Specific Energy (S.E.) $Whkg^{-1}$	260	40.05
Coulombic Efficiency (η) %	95	87

Graphical Abstract